


# Simple technique for determining the refractive index of phase-change materials using near-infrared reflectometry

E. GEMO,<sup>1</sup> S. V. KESAVA,<sup>2</sup> C. RUIZ DE GALARRETA,<sup>1</sup> L. TRIMBY,<sup>1</sup>  
S. GARCÍA-CUEVAS CARRILLO,<sup>1</sup> M. RIEDE,<sup>2</sup> A. BALDYCHEVA,<sup>1</sup> A.  
ALEXEEV,<sup>1</sup> AND C. D. WRIGHT<sup>1,\*</sup> 

<sup>1</sup>Department of Engineering, University of Exeter, Exeter EX4 4QF, UK

<sup>2</sup>Department of Physics, University of Oxford, Oxford OX1 3PU, UK

\*david.wright@exeter.ac.uk

**Abstract:** Phase-change materials, such as the well-known ternary alloy  $\text{Ge}_2\text{Sb}_2\text{Te}_5$ , are essential to many types of photonic devices, from re-writeable optical disk memories to more recent developments such as phase-change displays, reconfigurable optical metasurfaces, and integrated phase-change photonic devices and systems. The successful design and development of such applications and devices requires accurate knowledge of the complex refractive index of the phase-change material being used. To this end, it is common practice to rely on published experimental refractive index data. However, published values can vary quite significantly for notionally the same composition, no doubt due to variations in fabrication/deposition processes. Rather than rely on published data, a more reliable approach to index determination is to measure the properties of as-fabricated films, and this is usually carried out using specialized and dedicated ellipsometric equipment. In this paper, we propose a simple and effective alternative to ellipsometry, based on spectroscopic reflectance measurements of Fabry–Perot phase-change nanocavities. We describe this alternative approach in detail, apply it to measurement of the complex index of the archetypal phase-change materials  $\text{Ge}_2\text{Sb}_2\text{Te}_5$  and  $\text{GeTe}$ , and compare the results to those obtained using conventional ellipsometry, where we find good agreement.

Published by The Optical Society under the terms of the [Creative Commons Attribution 4.0 License](https://creativecommons.org/licenses/by/4.0/). Further distribution of this work must maintain attribution to the author(s) and the published article's title, journal citation, and DOI.

## 1. Introduction

Novel device technologies based on the use of chalcogenide phase-change materials (PCMs), whose refractive index can be controlled on-demand, are currently the subject of many fascinating research trends [1–4]. These include PCM-based reconfigurable reflective displays [1,3], tuneable filters [2], perfect absorbers/modulators [4], devices for active wavefront shaping [5], and integrated phase-change photonic memories and processors [6–8]. This is of course in addition to the use of PCMs in more conventional non-volatile optical (and electrical) memories (see e.g., [9,10]). A particularly well known and well explored PCM composition is the ternary alloy  $\text{Ge}_2\text{Sb}_2\text{Te}_5$  (or GST for short), which exhibits a high electro-optical contrast between amorphous and crystalline states (i.e., contrast in its complex refractive index and electrical resistivity), has fast switching times between states, can be switched between states hundreds of billions of times, and has excellent long-term stability [11–13]. However, in spite of GST's long history and ubiquity, its basic optical properties, i.e. its complex refractive index (index,  $n$ , and extinction coefficient,  $k$ ), as reported in the literature, suffer from a considerable degree of variability. For example, shown in Fig. 1 are two greatly differing data sets for the complex refractive index of GST in the near infrared (NIR), corresponding to the lower and higher bounds found in the literature [14,15]. Differences (between the two bounds) in the index  $n$  and extinction coefficient

$k$  of up to  $\Delta n_{am} = 1.2$  and  $\Delta k_{am} = 0.9$  can be seen for the amorphous phase of GST [Fig. 1(a)], and  $\Delta n_{cr} = 2.7$  and  $\Delta k_{cr} = 2.8$  for the crystalline phase [Fig. 1(b)].

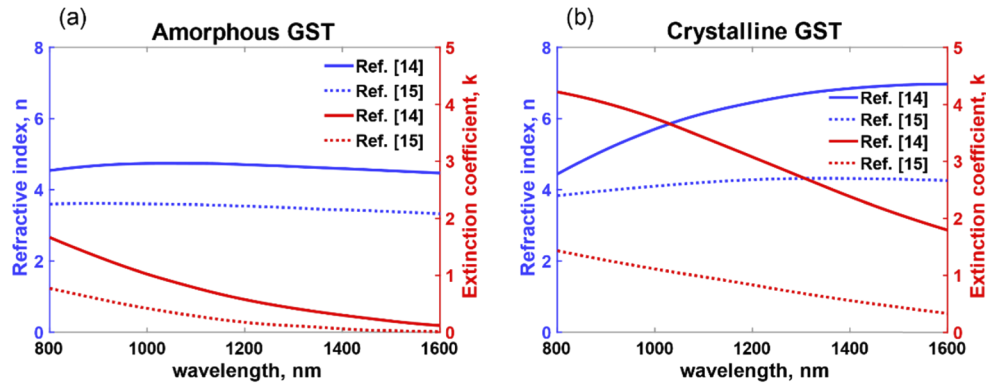


**Fig. 1.** Optical properties (complex refractive index) for (a) amorphous and (b) crystalline (fcc)  $\text{Ge}_2\text{Sb}_2\text{Te}_5$ , as reported in literature [14, 15]. Left axis (and blue lines) refers to the refractive index, whereas the right axis (and red lines) report the extinction coefficient. As visible, for the same material, the optical properties found in published data vary widely from reference to reference.

The origin of such a substantial difference in the reported  $n$  and  $k$  values, for notionally the same material, can no doubt be attributed to variations in fabrication/deposition conditions, which can have a significant effect on as-fabricated physical properties [16]. Such variations include differences in deposition rates, temperatures and pressures, aging of the target material, substrate material, layer thicknesses, surface properties, etc. [16–20]. Nevertheless, obtaining reliable data on the optical properties of as-fabricated PCM thin films is essential for the successful design, fabrication and characterization of photonic devices involving their use. Relying on published literature values, however, might not be the most accurate approach, as evidenced by the example of the variations in published data shown in Fig. 1 for GST. Ideally, the  $n$  and  $k$  values of PCM films should be evaluated for each new set of deposition conditions and for each deposition machine. Such an evaluation is traditionally carried out using ellipsometry, but such a methodology might not always be available. Alternative techniques do of course exist and, as in ellipsometry, most of them are based on retrieval of the optical amplitude and phase information from the sample under test, which are then used to obtain indirect  $n$  and  $k$  measurements via post-processing algorithms. For example, the combination of frequency-spectroscopy (which provides amplitude quantification) with interferometry (which allows measurement of optical phase) has been proposed as an accurate way to measure the refractive indices of thin films or liquids [21–24]. Other methods where the phase retrieval is accessible (such as time-domain spectroscopy) have also been employed successfully for the same purpose [25]. These techniques have shown good effectiveness, but in general require complex experimental setups and processing algorithms. On the other hand, frequency-domain spectroscopy by itself gives quantitative information about the amplitude of light absorbed, transmitted and reflected after interaction with a specimen, which directly depends on the  $n$  and  $k$  values of the sample under test. However, this technique provides amplitude quantification only, since the optical phase information is lost [22]. Such a lack of phase information makes the extraction of accurate complex refractive index data difficult, since multiple  $n$  and  $k$  solutions can reproduce the same reflectance/transmittance spectra. In this paper, therefore, we propose a simple but effective method to extract accurately the  $n$  and  $k$  values of thin PCM films, based on spectroscopic reflectance measurements. Restriction of multiple ( $n$  and  $k$ ) solutions is achieved by performing the measurements on structures forming

absorbing Fabry-Perot cavities, which possess unique key mapping features, i.e. reflectance at resonance, resonant wavelength  $\lambda_{res}$  and  $Q$  factor. Our analyses have been performed over thin films made of two different and very widely employed PCM compositions, namely  $\text{Ge}_2\text{Sb}_2\text{Te}_5$  (GST) and GeTe, working in the near infrared region of the spectrum (which is important for many emerging nanophotonic applications of PCMs (see e.g., [2–8]).

## 2. Background

Figure 2(a) displays the schematics of a simple Fabry-Perot (FP) cavity, here consisting of a tri-layer stack formed by a bottom metal plane, and a dielectric layer surrounded by air. The total reflected electric field,  $E_{out}$ , for an input electric field,  $E_{0m}$ , can be solved by superposing a series of secondary beams arising from internal reflections inside the cavity [22,26]:

$$E_{out} = \tilde{r} \cdot E_{0m} \quad (1a)$$

where  $E_0$  is the constant amplitude vector, and  $\tilde{r}$  is the (complex) reflection coefficient of the layer stack, whose value can be calculated employing the Fresnel-Airy formula (available in classic optics textbooks [26]), which for isotropic, non-magnetic materials and under normal incidence becomes, for both s- and p- polarizations,

$$\tilde{r} = \frac{\tilde{r}_{12} + \tilde{r}_{23} e^{i \frac{2\pi}{\lambda} t \tilde{n}_2}}{1 + \tilde{r}_{12} \tilde{r}_{23} e^{i \frac{2\pi}{\lambda} t \tilde{n}_2}} \quad (1b)$$

where  $\tilde{r}_{ij}$  are the complex-valued Fresnel reflection coefficients under normal incidence (i.e.,  $\tilde{r}_{ij} = (\tilde{n}_i - \tilde{n}_j)/(\tilde{n}_i + \tilde{n}_j)$ ),  $\lambda$  is the wavelength,  $t$  is the thickness of the dielectric layer and  $\tilde{n}_2$  its complex refractive index. As summarized in Fig. 2(b), the reflectance spectrum,  $R(\lambda) = |\tilde{r}(\lambda)|^2$ , of such a configuration is characterized by three key features: the  $Q$  factor, the resonant wavelength,  $\lambda_{res}$ , and the reflectance value at resonance,  $R(\lambda_{res})$ . In the case where  $\tilde{n}_2(\lambda)$  has moderate optical losses, the wavelength at which FP resonances occur can be approximated by the quarter-wave condition, due to reflection suppression arising from destructive interference originated by propagative phase accumulation inside the cavity [26–28]. This leads to the following relationship between the thickness  $t$  of the layer, the resonant wavelength and the refractive index:

$$t \approx \frac{\lambda_{res}}{4n_2} m \quad (2)$$

with  $m$  being an odd integer defining the FP resonance order.

In spite of the fact that information about the optical phase is lost when performing spectroscopy measurements, such FP key features ( $\lambda_{res}$ ,  $R(\lambda_{res})$  and  $Q = \lambda_{res}/\Delta\lambda$ ) are still mapped in the reflectance spectra, and depend exclusively on a unique value of the cavity complex refractive index,  $\tilde{n}_2(\lambda) = n_2(\lambda) + ik_2(\lambda)$ , assuming that the thickness of the layer  $t$  and the refractive indices of the surrounding materials ( $\tilde{n}_1(\lambda)$ ,  $\tilde{n}_3(\lambda)$ ) are known *a priori* [26]. Our proposed method to obtain the  $n$  and  $k$  values of PCM thin films is thus based around the uniqueness of the FP key features in the reflectance spectrum, which restricts the possible acquisition of multiple fitting solutions due to the lack of phase information. We obtain reflectance spectra for FP cavities containing thin films of the target (for  $n$  and  $k$  determination) phase-change material, and then fit to said reflectance spectrum using an algorithm that minimizes the fitting error. To restrict the search space, where published values of the refractive index are available for a particular PCM of interest, we use the maximum and minimum reported values of  $n$  and  $k$  to provide a truncated parametric search space (where such values are not available, reasonable estimates of maximum/minimum values can be used).

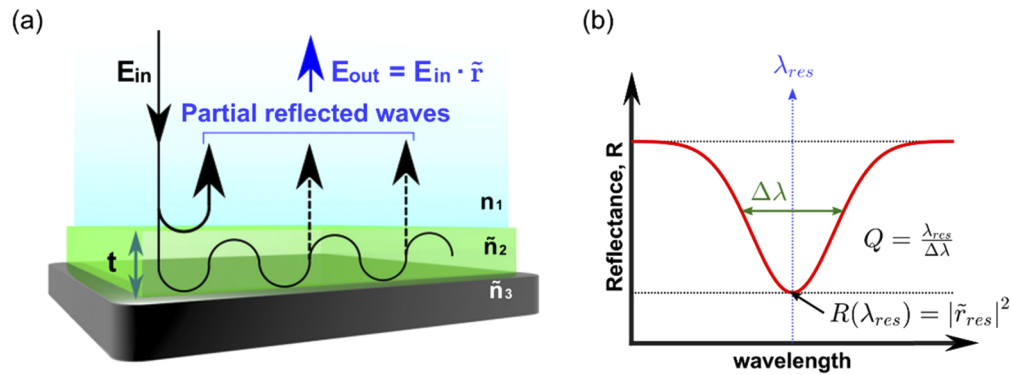


**Fig. 2.** (a) Diagram and interference working principle of a simple tri-layer Fabry-Perot cavity. (b) Characteristic features of a Fabry-Perot resonance which can be obtained via reflectance measurements, i.e. spectral position of resonance ( $\lambda_{res}$ ), reflectance at resonance ( $R(\lambda_{res})$ ), and  $Q$  factor.

### 3. Methods

Fabry-Perot tri-layer cavities, where here the three layers comprise an aluminium bottom layer, a GST or GeTe PCM layer, and a SiO<sub>2</sub> capping layer (which also protects the PCM layers from oxidation) were fabricated on Si substrates using magnetron sputtering (in an Ar atmosphere at a base pressure of 10<sup>-7</sup> mbar). Figures 3(a) and 3(b) show a schematic of the resulting layer stacks, consisting of thin films of the investigated materials lying on top of an optically thick (100 nm) reflective aluminium layer, and with a 10 nm SiO<sub>2</sub> top layer. We used aluminium for the bottom layer since it is often used for phase-change based optical metasurfaces (see e.g., Refs. [3,4,5]), and does not diffuse into, and alloy with, chalcogenides on heating (unlike Au for example). Any non-diffusive reflective metal would be suitable for this method however. Note that published data on the refractive index of GST and GeTe (specifically from [14]) was used to guide the choice of thickness of the PCM layers, using Eq. (2), to ensure that the FP resonance occurred in the spectral region of interest (here 800 to 1600 nm). In cases where such data is not available, samples with a range of PCM thicknesses might have to be fabricated, in order to ensure a resonance in the required wavelength range.

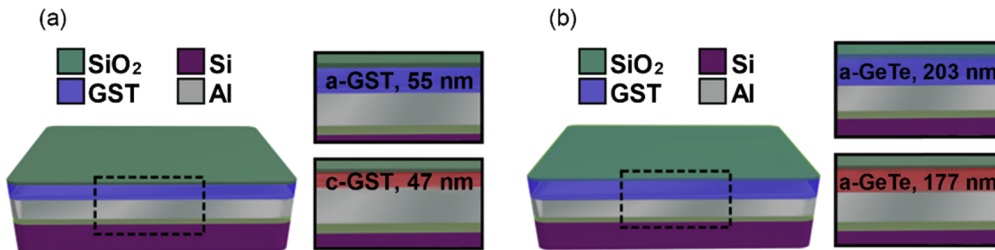


**Fig. 3.** Dimensions and materials of the fabricated cavities for (a) amorphous and crystalline GST and (b) amorphous and crystalline GeTe, all fabricated using magnetron sputtering on Si/SiO<sub>2</sub> substrates and capped by 10 nm SiO<sub>2</sub> layer.

Energy dispersive X-ray spectroscopy (EDS) measurements were performed on the as-sputtered films to confirm their correct composition after deposition. X-ray diffraction measurements (XRD) were made after fabrication (to corroborate that the as-sputtered films were in the

amorphous phase) and contact atomic force microscopy (AFM) scans were carried out to obtain the cavity thicknesses. Crystallization of the films was thermally induced via hot plate annealing at 200 °C for 10 minutes, and the phase transition (crystallinity of the layers) was confirmed afterward via further XRD measurements. Film thicknesses were re-measured after crystallization to account for any volume reduction [29] on switching from the amorphous to crystalline phase. The reflectance spectra of the GST and GeTe FP cavities were then measured over a wavelength range from 800 nm to 1600 nm using a JASCO 5300 micro-spectrophotometer. These measurements were normalized against a calibrated aluminium mirror of known reflectance, with the detector noise subtracted. The  $n$  and  $k$  values of the investigated PCM cavities (shown in Fig. 3) were then obtained by an iterative fitting approach, as described in detail below. Finally, the reliability/accuracy of our proposed Fabry-Perot reflectance spectroscopy method was assessed by comparison of the obtained refractive indices with those obtained from ellipsometry measurements over the same samples. Ellipsometry data was gathered using a J.A. Woollam M2000 ellipsometer at three different angles, 55°, 65° and 75°.

## 4. Results

### 4.1. Determination of $n$ and $k$ for $\text{Ge}_2\text{Sb}_2\text{Te}_5$

The measured reflectance spectra of the GST Fabry-Perot cavities for amorphous and crystalline phases are shown in Figs. 4(a) and 4(b). A FP absorbing resonance can be identified from the experimental results at  $\lambda_{res} \sim 1100$  nm for the amorphous phase [Fig. 4(a)] and  $\lambda_{res} \sim 1420$  nm [Fig. 4(b)] after crystallization, with the resonance of the crystalline phase being broadened (damped). The origin of such a spectral red-shift and damping is due to the characteristic increase of both the refractive index and the extinction coefficient of GST following crystallization. Also shown in the figures are simulated (using the transfer matrix method (TMM) [30]) reflectance spectra using published  $n$  and  $k$  data sets (taken here from Refs. [14] and [15], but other published data is also available, see e.g., [31,32]). Since reported  $n$  and  $k$  values for GST vary quite significantly, as already pointed out above, there is also a significant variation in the simulated reflectance spectra shown in Fig. 4, reinforcing the point that relying on published  $n$  and  $k$  data can be misleading and inappropriate.

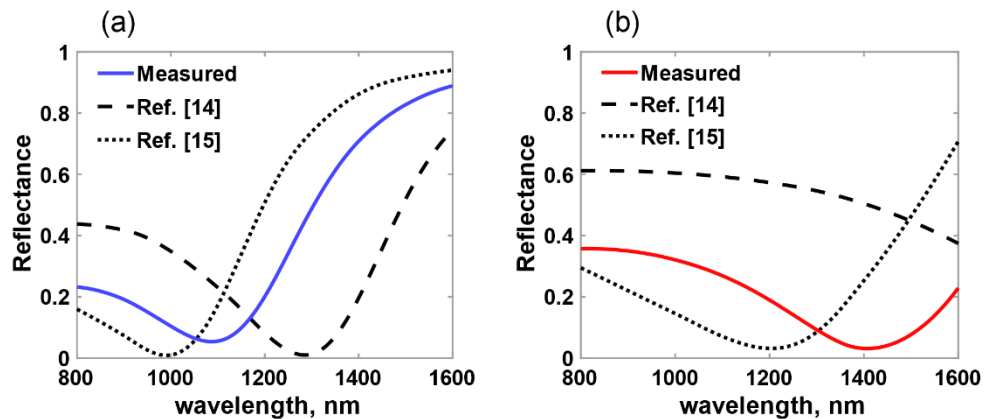


**Fig. 4.** Experimental reflectance spectra of GST Fabry-Perot cavities, compared to simulations using  $n$  and  $k$  values reported in references [14] and [15], with (a) the GST layer in the amorphous phase, and (b) in crystalline phase.

Also evident from Fig. 4 is the fact that the measured reflectance spectra lie completely within the reflectance range arising from simulated spectra, suggesting that the  $n$  and  $k$  values of the



GST films used to fabricate the FP cavities lie within the range of the values used to calculate the simulated spectra (i.e., within the range of values reported in Refs. [14] and [15] in this case). This allows us to use a truncated parametric search space for our  $k$  and  $n$  extraction algorithm. More specifically, we calculate the complex index  $\tilde{n}(\lambda)$  of the PCM films in this case via a weighted average of published values, using the equation

$$\tilde{n}(\lambda) = \sum_i^r w_i \tilde{n}_i(\lambda) \quad (3)$$

where  $w_i$  is the  $i^{\text{th}}$  reference weight (lying between 0 and 1) and  $\sum_i^r w_i = 1$  (we highlight that each  $w_i$  is applied to the whole  $\tilde{n}(\lambda)$  dispersion, i.e. the weights here are not dependent on  $\lambda$ ). The weights  $w_i$  are found by minimization of the mean-square error (MSE) between the measured and calculated reflectance spectra for the FP cavities. To minimize the MSE we used a pattern-search algorithm, due to its flexibility to span over multi-dimensional search spaces, its capability to avoid shallow local  $w_i$  solution minima (a merit of the convex objective function), and a relatively fast convergence time. In a little more detail, to find the  $\tilde{n}(\lambda)$  solution, we first generate a random weight set  $w_i$ , which yields a trial solution  $\tilde{n}(\lambda)$  from Eq. (3). The trial solution is used by the TMM solver, which outputs the related reflectance spectrum,  $R_{\text{calc}}(\lambda)$ . We then find the MSE according to:

$$MSE = \frac{1}{m} \sum_j^m (R_{\text{calc}}(\lambda_j) - R_{\text{exp}}(\lambda_j))^2 \quad (4)$$

where  $R_{\text{exp}}$  is the experimentally obtained reflectance spectrum. Equation (4) is then fed to the pattern-search algorithm as its objective function, to generate a new weight set in  $w_i$  Eq. (3), with the scope of minimizing the objective function output in an iterative process until a desired minimum MSE is reached. The complex refractive indices of the other materials in the cavities, i.e. and SiO<sub>2</sub> and Al, were taken from Refs. [33] and [34], and we note that only marginal differences in reported  $n$  and  $k$  values for these materials (of  $\Delta n = 1.5\%$  and  $\Delta k = 0.6\%$  within the spectral range of our analysis) are reported in the literature [33–38]. All calculations were performed using a regularly spaced selection of wavelengths, with a 5 nm step, as a finer stepping did not improve the fit quality. Note that a step-by-step guide and flowchart for the fitting algorithm is given in the appendix, and the code is available to download from [39].

We now present the results for GST for both amorphous and crystalline states. To obtain a suitable  $n(\lambda)$  and  $k(\lambda)$  solution, we here restricted the search space to the maximum and minimum values in  $n$  and  $k$  reported in Refs. [14] and [15] (but note that instead of literature values reasonable estimates can be made of the likely maximum/minimum range in which  $n$  and  $k$  will be found). Figures 5(a) and 5(b) show the resulting extracted values of  $n$  and  $k$  for the amorphous phase. Also shown in the figures are the  $n$  and  $k$  values determined by our own direct ellipsometric measurements of our samples, revealing excellent agreement between values extracted by fitting to the reflectance spectra and those from ellipsometry (note that the MSE in  $\Psi$  and  $\Delta$  for our ellipsometric measurements was small, always less than 5). Indeed to quantify the level of agreement between these two cases we find the average error for  $n$  ( $\Delta n$ ) and  $k$  ( $\Delta k$ ) and the relative error,  $\zeta$ , which we define as:

$$\zeta(q, \lambda) = \left| \frac{(q_r(\lambda) - q_{el}(\lambda))}{q_{el}(\lambda)} \right| \quad (5)$$

with  $q_r = (n_r, k_r)$  being the estimation and  $q_{el} = (n_{el}, k_{el})$  referring to the ellipsometrically measured parameters. Thus, for the cases of Figs. 5(a) and 5(b) the average and relative errors are respectively  $\Delta n = 0.021$ ,  $\bar{\zeta}(n) = 0.55\%$  and  $\Delta k = 0.017$ ,  $\bar{\zeta}(k) = 6.85\%$ , over the wavelength range shown. Finally, in Fig. 5(c) we plot the measured amorphous reflectance spectrum and

compare it to simulations using  $n$  and  $k$  values obtained numerically, and those obtained by our own ellipsometric measurements. In both cases we obtain a much better fit than that obtained using literature values [14,15] for  $n$  and  $k$  (MSE of 0.0018 *cf.* of 0.095 and 0.0281 for reflectance calculated using reference datasets).

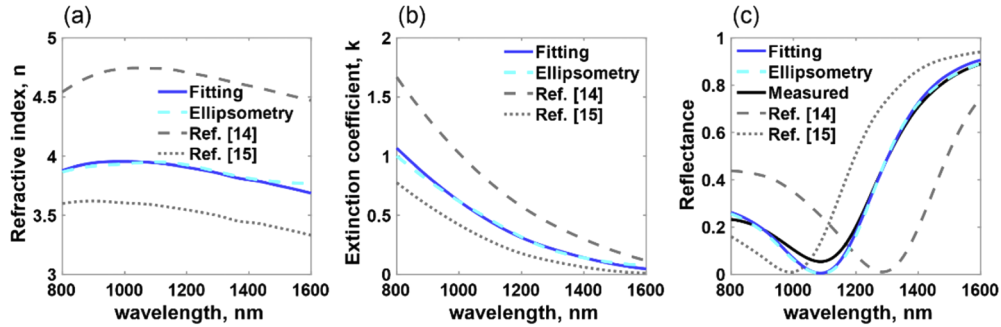


**Fig. 5.** (a-b) Refractive index (a) and extinction coefficient (b) for our amorphous GST, obtained with our simple method (blue solid lines) and compared to our ellipsometry measurements (blue dashed lines) and literature values from Refs. [14, 15] (grey lines). (c) Measured reflectance spectrum for amorphous GST (black line) against simulated spectra employing  $n$  and  $k$  values obtained from our simple method (blue solid line), from our ellipsometry measurements (blue dashed line) and from literature (grey lines) [14, 15].

The equivalent results to those of Fig. 5 but for the crystalline phase of GST are shown in Fig. 6. In line with the previous fitting for amorphous GST, a good agreement is apparent between the values for  $n$  [Fig. 6(a)] and  $k$  [Fig. 6(b)] obtained via fitting to reflectance spectra and those from our own ellipsometric measurements (in this case  $\Delta n = 0.18$ ,  $\bar{\zeta}(n) = 4.54\%$  and  $\Delta k = 0.19$ ,  $\bar{\zeta}(k) = 25.1\%$ ). The corresponding reflectance spectra are shown in Fig. 6(c), where again the agreement is good between the measured spectrum and that simulated using  $n$  and  $k$  values obtained numerically and from our own ellipsometric measurements (MSE of 0.0059), but rather poor in the case of literature values [14,15] (MSE of 0.12 and 0.056 respectively).

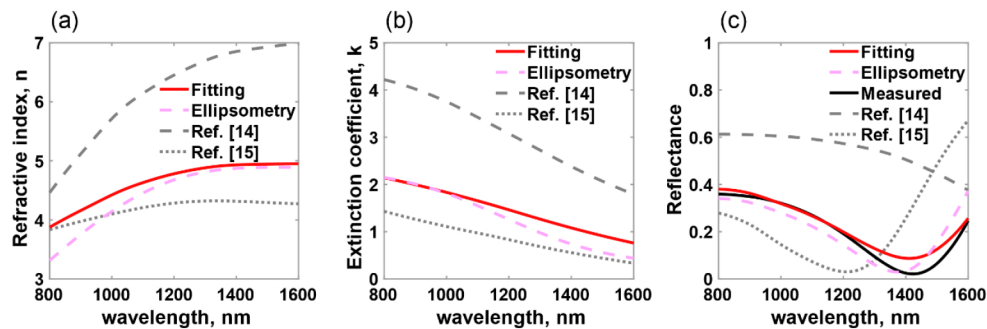


**Fig. 6.** (a-b) Refractive index (a) and extinction coefficient (b) for our crystalline GST, obtained with our simple method (red solid lines) and compared to our ellipsometry measurements (pink dashed lines) and literature values from Refs. [14, 15] (grey lines). (c) Measured reflectance spectrum for crystalline GST (black line) against spectra simulated using  $n$  and  $k$  values obtained from our simple method (red solid line), from our ellipsometry measurements (pink dashed lines) and from literature (grey lines) [14, 15].

#### 4.2. Determination of $n$ and $k$ for GeTe

Having demonstrated above the efficacy of our proposed method for the determination of the  $n$  and  $k$  values for  $\text{Ge}_2\text{Sb}_2\text{Te}_5$  from the reflectance spectra of Fabry-Perot nanocavities, we now apply the same approach for probably what is the next most common/well-known phase-change chalcogenide, namely GeTe. The FP cavity structure in this case was shown previously in Fig. 3(b), and the solution space for  $n$  and  $k$  was this time truncated by employing maximum and minimum values of  $n$  and  $k$  from Refs. [14] and [40] respectively.

Results in this case are shown in Fig. 7 and Fig. 8. Figures 7(a) and 7(b) show  $n$  and  $k$  for amorphous GeTe, as determined using fitting to the FP reflectance spectrum, from our own ellipsometry measurements and from Refs. [14] and [40]. Again, the values extracted from the FP spectrum agree well with those obtained by our own ellipsometric measurements (the average error in this case being  $\overline{\Delta n} = 0.14$  ( $\bar{\zeta}(n) = 3.57\%$ ) and  $\overline{\Delta k} = 0.043$  ( $\bar{\zeta}(k) = 13.7\%$ )), but differ from the literature values. As would be expected, the FP reflectance spectrum simulated using the  $n$  and  $k$  values obtained by fitting, see Fig. 7(c), matches well with the experimentally obtained spectrum (with a MSE value of 0.0003), unlike the spectra simulated using literature values (which indeed have MSE values of 0.055 and 0.062).

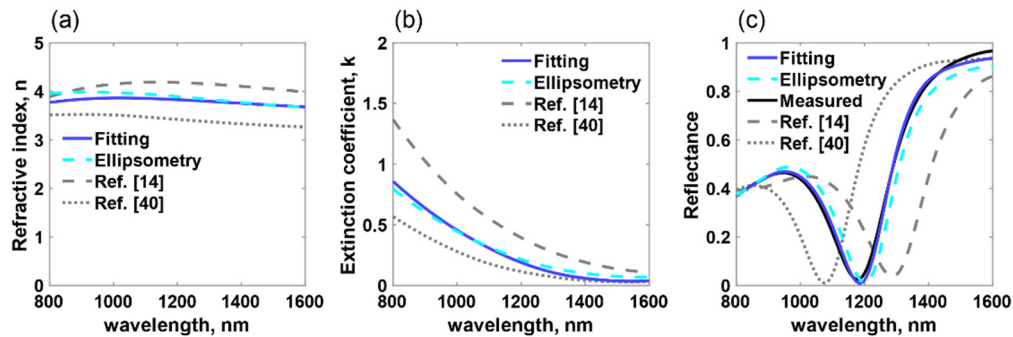


**Fig. 7.** (a-b) Refractive index (a) and extinction coefficient (b), for our amorphous GeTe obtained with our simple method (blue solid lines) and compared to our ellipsometry measurements (blue dashed lines) and literature values from Refs. [14, 40] (grey lines). (c) Measured reflectance spectrum for amorphous GeTe (black solid line) against spectra simulated using  $n$  and  $k$  values obtained from our method (blue solid line), from our ellipsometry measurements (blue dashed line) and from literature (grey lines) [14, 40].

Finally, results obtained from crystalline GeTe films are displayed in Fig. 8, with Figs. 8(a) and 8(b) showing  $n$  and  $k$  extracted from FP spectra, from our own ellipsometric measurements and from Refs. [14] and [40]. The agreement between FP-extracted values and our ellipsometry values is not quite so good in this case [calculated average errors are  $\overline{\Delta n} = 0.20$  ( $\bar{\zeta}(n) = 3.21\%$ ) and  $\overline{\Delta k} = 0.18$  ( $\bar{\zeta}(k) = 41.3\%$ )], but again is much better than that with GeTe literature values. The slightly less good fitting in this case of  $n$  and  $k$  values also leads, as would be expected, to a less good fit between simulated and experimental FP reflectance spectra, as shown in Fig. 8(c), which has an MSE of 0.0057. A closer agreement can be obtained by use of a wavelength-dependent weight  $w(\lambda)$  fitting (interpolated by use of a 3<sup>rd</sup> order polynomial function) in combination with the prioritising of fitting of weights around the resonant FP wavelength (the latter being done by relaxing the constraints imposed by the literature values of  $n$  and  $k$ ). Such an alternative fitting is also shown in Fig. 8 (green lines), where the agreement with our own ellipsometric data is significantly improved around the resonance wavelength (though deviates away from resonance).



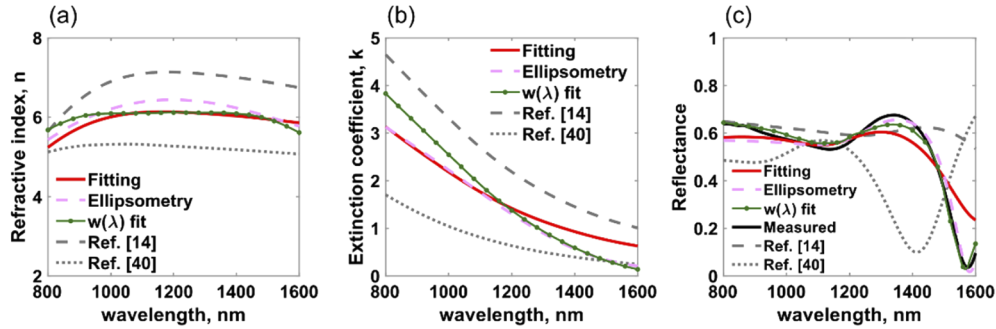


**Fig. 8.** (a-b) Refractive index (a) and extinction coefficient (b), for our crystalline GeTe, obtained with our simple method (red and green solid lines) and compared to our ellipsometry measurements (pink dashed lines) and literature values from Refs. [14, 40] (grey lines). (c) Measured reflectance spectrum (black solid line) against spectra simulated using  $n$  and  $k$  values obtained from our method (red and green solid lines), from our ellipsometry measurements (pink dashed lines) and from literature (grey lines) [14, 40]. (Note that the green lines shows results from the wavelength-dependent weight fitting approach, that prioritises fitting at resonance).

## 5. Discussion and conclusions

We have demonstrated a way of determining, with a good degree of accuracy, the complex refractive index of phase-change materials without the need for ellipsometry equipment and/or complicated post-processing algorithms. The proposed methodology is based on simple reflectance measurements of thin films forming Fabry–Perot absorbing nanocavities; this restricts multiple ( $n$  and  $k$ ) solutions, since the FP cavities possess unique mapping features (reflectance at resonance, resonant wavelength  $\lambda_{res}$  and  $Q$  factor). Although here we have concentrated on the determination of  $n$  and  $k$  values over the near infrared spectral region, the method is extendable to the visible, mid- and long-wave infrared red regions (where phase-change materials have many interesting applications, see e.g., [1–3,9,15,41]), the only proviso being that the nanocavities used (designed) should have a resonance in the relevant wavelength range.

Our proposed approach has been validated against ellipsometry measurements, and replicated using two of the most common, well-known and technologically important chalcogenide phase-change materials, namely  $\text{Ge}_2\text{Sb}_2\text{Te}_5$  and GeTe. The foundation of our method lays in the calculation of the refractive index through a purposely built optimization routine, which finds the closest solution based on a linear combination of maximum and minimum literature data to provide a truncated parametric search space (in cases where such data does not exist, reasonable assumptions of the likely maximum/minimum ranges of  $n$  and  $k$  can be used instead). In addition, the proposed algorithm provides a self-validation routine, as it is based on matching the experimentally obtained FP reflectance spectra to theoretical spectra calculated via iteratively obtained  $n$  and  $k$  values. Refractive index data obtained using our approach was found to be in good agreement (low mean-square-error) with those obtained from ellipsometry measurements of the same samples. Further improvement of the proposed methodology could be made via performing wavelength-by-wavelength fittings within the solution space.

In conclusion, we believe that the herein proposed work can be used to obtain, and/or increase the accuracy of, the  $n$  and  $k$  values of as-fabricated PCM thin films, without the need of expensive ellipsometry equipment. Our method could be also used for characterization of other (non-phase-change) materials, provided that literature values are available to create a solution space, or that reasonable estimates can be made of the likely maximum/minimum range in which

$n$  and  $k$  will be found. This could be therefore a useful tool for researchers working in the general field of nanophotonics and optical thin films.

## Appendix

We here summarize each step of algorithm for determination of  $n$  and  $k$  using the approach described in Sec. 4.1 of the main text.

Step 1: Generate a random weight set  $w_i$ , with  $\sum_i w_i = 1$  (as many weights as references)

Step 2: Construct a test index  $\tilde{n}(\lambda)$ , as  $\tilde{n}(\lambda) = \sum_i w_i \tilde{n}_i(\lambda)$

Step 3: Calculate the cavity reflectance  $R$ , via TMM, including the test index  $\tilde{n}(\lambda)$

Step 4: Compare the calculated and experimental reflectance spectra by building the mean square error:  $MSE = \frac{1}{m} \sum_j^m (R_{calc}(\lambda_j) - R_{exp}(\lambda_j))^2$

Step 5: If the MSE is arbitrarily small (i.e. lower than a value set by the user), the solution is found; otherwise, the algorithm returns to Step 1 and generates an improved  $w_i$  set via pattern-search method.

A flowchart for the above algorithm is also provided in Fig. 9.

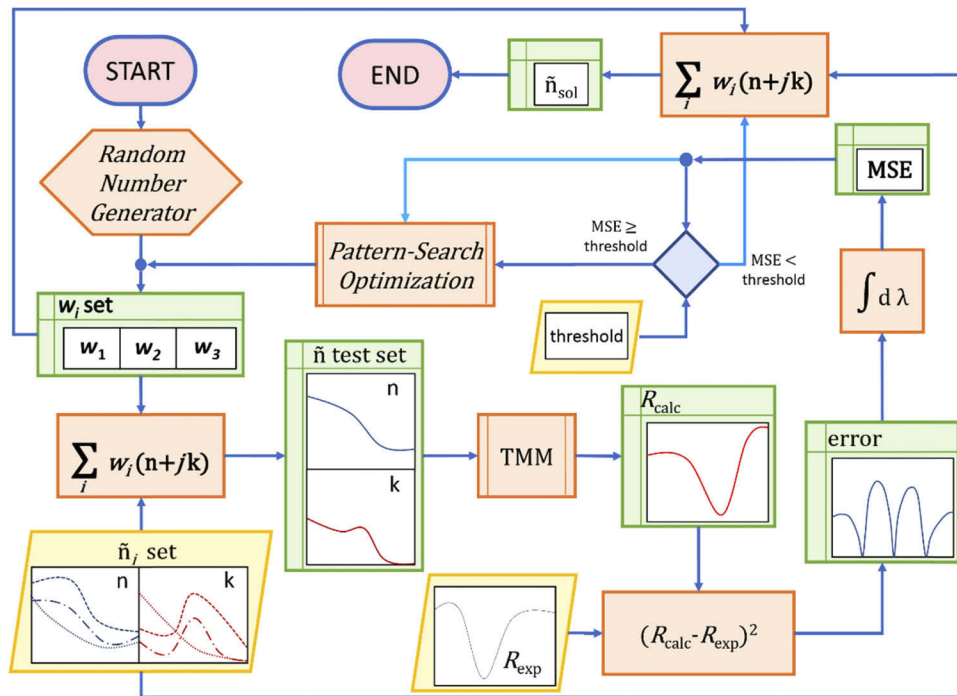


Fig. 9. Flowchart describing the method for determination of  $n$  and  $k$ .

## Author Contributions

C.R.G., A.A. and C.D.W conceived the study. C.R.G. and L.T. carried out the fabrication steps, with help from S.G.C.C., A.A., and E.G. AFM and reflectometric analysis have been performed by C.R.G. and L.T. XRR verification has been carried out by S.G.C.C and E.G. S.V.K and L.T. measured and analyzed the ellipsometric data. E.G. implemented the simulation framework with contributions from L.T. The manuscript was written by C.R.G., E.G., L.T. and C.D.W., and all authors participated in the manuscript review.

## Funding

Engineering and Physical Sciences Research Council (EP/L015331/1, EP/M015130/1, EP/M015173/1); Horizon 2020 Framework Programme (780848); START (ST/R002754/1).

## Acknowledgments

We acknowledge funding for this work from the EPSRC WAFT Collaboration (EP/M015173/1); the EPSRC Chalcogenide Advanced Manufacturing Partnership (ChAMP) (EP/M015130/1); the EU Horizon 2020 research and innovation program (780848, FunCOMP project); the EPSRC CDT in Metamaterials (EP/L015331/1); the Synchrotron Techniques for African Research and Technology (START) (ST/R002754/1).

## Disclosures

The authors declare no conflicts of interest.

## Data Availability

Data relating to this manuscript can be obtained from the authors.

## References

1. P. Hosseini, C. D. Wright, and H. Bhaskaran, "An optoelectronic framework enabled by low-dimensional phase-change films," *Nature* **511**(7508), 206–211 (2014).
2. M. Wuttig, H. Bhaskaran, and T. Taubner, "Phase-Change materials for non-volatile photonic applications," *Nat. Photonics* **11**(8), 465–476 (2017).
3. S. García-Cuevas Carrillo, L. Trimby, Y.-Y. Au, K. Nagareddy, G. Rodriguez-Hernandez, P. Hosseini, C. Rios, H. Bhaskaran, and C. D. Wright, "A Nonvolatile Phase-Change Metamaterial Color Display," *Adv. Opt. Mater.* **7**(18), 1801782 (2019).
4. S. García-Cuevas Carrillo, A. M. Alexeev, Y.-Y. Au, and C. D. Wright, "Reconfigurable phase-change meta-absorbers with on-demand quality factor control," *Opt. Express* **26**(20), 25567–25581 (2018).
5. C. Ruiz de Galarreta, A. M. Alexeev, Y.-Y. Au, M. Lopez-Garcia, M. Klemm, M. Cryan, J. Bertolotti, and C. D. Wright, "Nonvolatile reconfigurable phase-change metadevices for beam steering in the near infrared," *Adv. Funct. Mater.* **28**(10), 1704993 (2018).
6. E. Gemo, S. García-Cuevas Carrillo, C. Ruiz De Galarreta, A. Baldycheva, H. Hayat, N. Youngblood, H. Bhaskaran, W. H. P. Pernice, and C. D. Wright, "Plasmonically-enhanced all-optical integrated phase-change memory," *Opt. Express* **27**(17), 24724–24737 (2019).
7. J. Feldmann, N. Youngblood, C. D. Wright, H. Bhaskaran, and W. H. P. Pernice, "All-optical spiking neurosynaptic networks with self-learning capabilities," *Nature* **569**(7755), 208–214 (2019).
8. C. Ríos, N. Youngblood, Z. Cheng, M. Le Gallo, W. H. P. Pernice, C. D. Wright, A. Sebastian, and H. Bhaskaran, "In-memory computing on a photonic platform," *Sci. Adv.* **5**(2), eaau5759 (2019).
9. M. Wuttig and N. Yamada, "Phase-change materials for rewriteable data storage," *Nat. Mater.* **6**(11), 824–832 (2007).
10. G. W. Burr, S. Kim, M. Brightsky, A. Sebastian, H.-L. Lung, H.-Y. Cheng, N. E. S. Cortes, J. Y. Wu, H. Pozidis, and C. Lam, "Recent progress in Phase change memory technology," *IEEE J. Emerg. Sel. Topics Circuits Syst.* **6**(2), 146–162 (2016).
11. D. Loke, T. H. Lee, W. J. Wang, L. P. Shi, R. Zhao, Y. C. Yeo, T. C. Chong, and S. R. Elliott, "Breaking the speed limits of phase-change memory," *Science* **336**(6088), 1566–1569 (2012).
12. J. Siegel, C. N. Afonso, and J. Solis, "Dynamics of ultrafast reversible phase transitions in GeSb films triggered by picosecond laser pulses," *Appl. Phys. Lett.* **75**(20), 3102–3104 (1999).
13. W. Kim, M. Brightsky, T. Masuda, N. Sosa, S. Kim, R. Bruce, F. Carta, G. Fraczak, H. Y. Cheng, A. Ray, Y. Zhu, H. L. Lung, K. Suu, and C. Lam, "ALD-based confined PCM with a metallic liner toward unlimited endurance," *IEDM Tech. Dig.*, 4.2.1–4.2.4 (2016).
14. K. Shportko, S. Kremers, M. Woda, D. Lencer, J. Robertson, and M. Wuttig, "Resonant bonding in crystalline phase-change materials," *Nat. Mater.* **7**(8), 653–658 (2008).
15. B. Gholipour, J. Zhang, K. F. MacDonald, D. W. Hewak, and N. I. Zheludev, "An all-optical, non-volatile, bidirectional, phase-change meta-switch," *Adv. Mater.* **25**(22), 3050–3054 (2013).
16. H. Dieker and M. Wuttig, "Influence of deposition parameters on the properties of sputtered Ge<sub>2</sub>Sb<sub>2</sub>Te<sub>5</sub> films," *Thin Solid Films* **478**(1-2), 248–251 (2005).
17. T. Welzel and K. Ellmer, "The influence of the target age on laterally resolved ion distributions in reactive planar magnetron sputtering," *Surf. Coat. Technol.* **205**(2), S294–S298 (2011).

18. J. Aarik, A. Aidla, A.-A. Kiisler, T. Uustare, and V. Sammelseg, "Influence of substrate temperature on atomic layer growth and properties of HfO<sub>2</sub> thin films," *Thin Solid Films* **340**(1-2), 110–116 (1999).
19. W. Rieger, T. Metzger, H. Angerer, R. Dimitrov, O. Ambacher, and M. Stutzmann, "Influence of substrate-induced biaxial stress on the optical properties of thin GaN films," *Appl. Phys. Lett.* **68**(7), 970–972 (1996).
20. M. Bender, W. Seeling, C. Daube, H. Frankenberger, B. Ocker, and J. Stollenwerk, "Dependence of film composition and thicknesses on optical and electrical properties of ITO-metal-ITO multilayers," *Thin Solid Films* **326**(1-2), 67–71 (1998).
21. Y. Zang, J. B. Chou, J. Li, H. Li, Q. Du, A. Yadav, S. Zhou, M. Y. Shalaginov, Z. Fang, H. Zhong, and C. Roberts, "Extreme Broadband Transparent Optical Phase Change Materials for High-Performance Nonvolatile Photonics," arXiv preprint arXiv:1811.00526 (2018).
22. M. Born and E. Wolf, *Principles of Optics: Electromagnetic Theory of Propagation, Interference and Diffraction of Light* (Elsevier, 2013).
23. Z. Bor, K. Osvey, B. Racz, and G. Szabo, "Group refractive index measurement by Michelson interferometer," *Opt. Commun.* **78**(2), 109–112 (1990).
24. P. Hlubina, "White light spectral interferometry with the uncompensated Michelson interferometer and the group refractive index dispersion in fused silica," *Opt. Commun.* **193**(1-6), 1–7 (2001).
25. L. Duvillearet, F. Garet, and J. L. Coutaz, "A Reliable Method for Extraction of Material Parameters in Terahertz Time-Domain Spectroscopy," *IEEE J. Sel. Top. Quantum Electron.* **2**(3), 739–746 (1996).
26. H. A. Macleod, *Thin-Film Optical Filters*, 4 Edition (CRC Press, 2010).
27. A. Kats and F. Capasso, "Optical absorbers based on strong interference in ultra-thin films," *Laser Photonics Rev.* **10**(5), 735–749 (2016).
28. M. A. Kats, R. Blanchard, P. Genevet, and F. Capasso, "Nanometre optical coatings based on strong interference effects in highly absorbing media," *Nat. Mater.* **12**(1), 20–24 (2013).
29. T. P. Leervad Pedersen, J. Kalb, W. K. Njoroge, D. Wamwangi, and M. Wuttig, "Mechanical stresses upon crystallisation in phase change materials," *Appl. Phys. Lett.* **79**(22), 3597–3599 (2001).
30. R. C. Rumpf, "Improved formulation of scattering matrices for semi-analytical methods that is consistent with convention," *Prog. Electromagn. Res. B* **35**, 241–261 (2011).
31. C. Wu, H. Yu, H. Li, X. Zhang, I. Takeuchi, and M. Li, "Low-Loss Integrated Photonic Switch Using Subwavelength Patterned Phase Change Material," *ACS Photonics* **6**(1), 87–92 (2019).
32. W. H. P. Pernice and H. Bhaskaran, "Photonic non-volatile memories using phase change materials," *Appl. Phys. Lett.* **101**(17), 171101 (2012).
33. I. H. Malitson, "Interspecimen comparison of the refractive index of fused silica," *J. Opt. Soc. Am.* **55**(10), 1205–1208 (1965).
34. A. D. Rakić, "Algorithm for the determination of intrinsic optical constants of metal films: application to aluminum," *Appl. Opt.* **34**(22), 4755–4767 (1995).
35. A. G. Mathewson and H. P. Myers, "Absolute values of the optical constants of some pure metals," *Phys. Scr.* **4**(6), 291–292 (1971).
36. L. Gao, F. Lemarchand, and M. Lequime, "Exploitation of multiple incidences spectrometric measurements for thin film reverse engineering," *Opt. Express* **20**(14), 15734–15751 (2012).
37. M. A. Green, "Self-consistent optical parameters of intrinsic silicon at 300K including temperature coefficients," *Sol. Energy Mater. Sol. Cells* **92**(11), 1305–1310 (2008).
38. A. D. Rakić, A. B. Djurišić, J. M. Elazar, and M. L. Majewski, "Optical properties of metallic films for vertical-cavity optoelectronic devices," *Appl. Opt.* **37**(22), 5271–5283 (1998).
39. <https://github.com/EmanueleGemo/algorithm-for-n-k-determination-from-reflectance-spectra>
40. M. Jafari and M. Rais-Zadeh, "Zero-static-power phase-change optical modulator," *Opt. Lett.* **41**(6), 1177–1180 (2016).
41. Y. Qu, Q. Li, L. Cai, M. Pan, P. Ghosh, K. Du, and M. Qiu, "Thermal camouflage based on the phase-changing material GST," *Light: Sci. Appl.* **7**(1), 1–10 (2018).